Nanocrystalline SnO_2-Based Thin Films Obtained by Sol−Gel Route: A Morphological and Structural Investigation

M. Acciarri, C. Canevali, C. M. Mari, M. Mattoni, R. Ruffo, R. Scotti, and F. Morazzoni*

INSTM and Dipartimento di Scienza dei Materiali, Università degli Studi di Milano-Bicocca, via Cozzi 53, 20125 Milano, Italy

D. Barreca, L. Armelao, and E. Tondello

Istituto di Scienze e Tecnologie Molecolari del CNR and INSTM, Dipartimento di Chimica, Università di Padova, Via Marzolo, 1, 35131 Padova, Italy

E. Bontempi and L. E. Depero

INSTM and Laboratorio di Strutturistica Chimica, Dipartimento di Ingegneria Meccanica, Università di Brescia, Via Branze 38, 25123 Brescia, Italy

Received January 8, 2003. Revised Manuscript Received March 17, 2003

The thermal evolution of sol−gel SnO_2-based thin films was explored by investigating their structural and morphological features. Nanostructured SnO_2 and Pt-doped SnO_2 layers were obtained using tetra(*tert*-butoxy)tin(IV) and Pt(II) acetylacetonate as precursors. Films were prepared by spin coating from ethanol solutions with different viscosity. After drying at room temperature, they were annealed in air at 673 and 973 K. The surface morphology was analyzed by scanning electron microscopy, atomic force microscopy, and scanning near-field optical microscopy. The structural characterization was performed by means of glancing incidence X-ray diffraction and microdiffraction. Both drying at room temperature and thermal treatment at 673 K resulted in the formation of holes on the surface and inside the films. Their distribution and average dimension were found to depend mainly on the viscosity of the sol precursor, and on the presence of Pt in the films. After annealing at 973 K, surface segregation of PtO_x phases and partial filling of the surface holes occurred. The effects of morphology on the electrical transport properties are discussed on the basis of sensitivity, S, measurements ($S = R_{air}/R_{CO}$, where R_{air} and R_{CO} stand for the resistance in air and CO/air, respectively).

Introduction

Tin dioxide-based films have attracted increasing scientific interest due to their extensive applications in solid-state sensing devices for reducing gases, for example, CO, NO, C_2H_5OH, and CH_4.[1−6] The detecting efficiency of such semiconductor oxide materials is based on the changes of their electrical properties that are mainly determined by point defects distribution, elemental composition, structure, and microstructure of the films.[1,2,7] In particular, gas−film interactions that are responsible for electrical properties changes largely depend on oxygen defect distribution and on chemisorbed oxygen species. As a matter of fact, in the case of nanostructured coatings, such interaction may result in improved system performances thanks to the high surface-to-volume ratio.[8] Furthermore, gas sensors with enhanced stability, sensitivity, and improved selectivity toward specific gases can be developed by doping pure SnO_2 with noble metals, for example, Pt and Pd.[9−13] Nevertheless, despite the reported enhancement in SnO_2 film performances due to the presence of such

* Corresponding author. E-mail: franca.morazzoni@mater.unimib.it. Fax: 39-02-64485400.

(1) Shimizu, Y.; Egashira, M. *MRS Bull.* **1999**, *24* (6), 18−24 and references therein.
(2) Schierbaum, K. D.; Weimar, U.; Göpel, W.; Kowalkowski, R. *Sensors Actuators B* **1991**, *3*, 205−214.
(3) Ansari, S. G.; Boroojerdian, P.; Sainkar, S. R.; Karekar, R. N.; Aiyer, R. C.; Kulkarni, S. K. *Thin Solid Films* **1997**, *295*, 271−276.
(4) Jin, Z.; Zhou, H. J.; Jin, Z. L.; Savinell, R. F.; Liu, C. C. *Sensors Actuators B* **1998**, *52*, 188−194.
(5) Schweizer-Berberich, M.; Zheng, J. G.; Weimar, U.; Göpel, W.; Bârsan, N.; Pentia, E.; Tomescu, A. *Sensors Actuators B* **1996**, *31*, 71−75.
(6) Varghese, O. K.; Mahlotra, L. K.; Sharma, G. L. *Sensors Actuators B* **1999**, *55*, 161−165.
(7) Sangaletti, L.; Depero, L. E.; Allieri, B.; Pioselli, F.; Comini, E.; Sberveglieri, G.; Zocchi, M. *J. Mater. Res* **1998**, *13*, 2457 and references therein.
(8) Yamazoe, N.; Miura, N. In *Chemical Sensor Technology*; Yamauchi, S., Ed.; Elsevier: New York, 1992; Vol. 4, p 19.
(9) Duh, J. G.; Jou, J. W.; Chiou, B. S *J. Electrochem. Soc.* **1989**, *136*, 2740.
(10) Matsushima, S.; Teraoka, Y.; Miura, N.; Yamazoe, N. *Jpn. J. Appl. Phys.* **1989**, *27*, 1798.
(11) Matko, I.; Gaidi, M.; Hazemann, J. L.; Chenevier, B.; Labeau, M. *Sensors Actuators B* **1999**, *59*, 210−215.
(12) Cheong, H. W.; Choi, J. J.; Kim, H. P.; Kim, J. M.; Churn, G. S. *Sensors Actuators B* **1992**, *9*, 227−231.
(13) Tadeev, A. V.; Delabouglise, G.; Labeau, M. *Mater. Sci. Eng. B* **1998**, *57*, 76−83.

10.1021/cm031002w CCC: $25.00
Published on Web 05/31/2003

dopants, little information is available about the physical and chemical origin of the observed effects. To this regard, a detailed study of the role played by the noble metal on the sensing mechanisms was reported in previous papers which focused on nanostructured metal-doped SnO_2 samples prepared both as powders and as thin films.[14,15]

Recent studies[16] showed that, besides nanostructural and compositional features, the surface morphology plays a key role in modifying the sensing activity of the films.

On this basis, a thorough investigation of the relationships between structure, composition, morphology, and electrical properties is of outstanding importance to develop devices with tailored performances. To our knowledge, only few detailed studies concerning the morphology of noble metal-doped SnO_2 are available in the literature,[17] mainly addressed to study polycrystalline materials, rather than thin films.

Different techniques have been employed to obtain pure and doped SnO_2 layers such as chemical vapor deposition,[18−20] aerosol pyrolysis,[11,13] magnetron sputtering,[21,22] physical vapor deposition,[5,17] and laser ablation.[23] In comparison to them, the sol−gel route[4,6,24−29] represents a low-temperature and low-cost approach to the solid state, thus allowing a fine control on the composition, microstructure, and morphology of the obtained layers.[30] We have recently reported a novel sol−gel route to synthesize Pt-doped nanocrystalline SnO_2 thin films for gas sensors,[15] focusing the attention on their structural and electronic properties. The present paper prosecutes the previous studies with the aim of elucidating the combined effects of composition and morphology on the electrical performances of SnO_2-based films for CO detection.

The morphology of the films obtained by solutions with different viscosity is discussed. The analysis was performed by comparing the results obtained by scanning electron microscopy (SEM) and atomic force microscopy (AFM) with those of scanning near-field optical microscopy (SNOM). While the more common electron and atomic force microscopy experiments were performed to study the surface topography and to evaluate the average film roughness, the SNOM technique[31,32] simultaneously yields separate optical and topographical images.

The film structure and microstructure were investigated by glancing incidence X-ray diffraction (GIXRD) and microdiffraction (micro-XRD) experiments.

The results evidence the effects on the film morphology induced by (i) different viscosity of the sol precursor, (ii) doping with a given transition metal content (Pt: SnO_2 0.025 molar ratio), and (iii) annealing in air at increasing temperature (673 K, 973 K).

A correlation between the surface topography of the films and their electrical transport properties is proposed.

Experimental Section

Film Preparation. Pure and Pt-doped SnO_2 films with 0.025 Pt:SnO_2 molar ratio were prepared.

$[Sn(OBu^t)_4]$ was chosen as the Sn precursor and prepared according to the literature,[33] while $[Pt(acac)_2]$ was used as the Pt source, purchased from Aldrich, and employed without further purification. The sol phase was prepared under a nitrogen atmosphere by mixing 2.50 mL of a $[Sn(OBu^t)_4]$ solution (360 mg/mL) in absolute anhydrous ethanol (2.19 mmol of Sn) with 3.00 mL of a $[Pt(acac)_2]$ solution (7.17 mg/mL) in ethanol−acetylacetone 1:1 v:v (5.47×10^{-2} mmol of Pt). After a few minutes, 1.00 mL (11.0 mmol of H_2O) of an ethanol−water solution, 4:1 v:v, was added and the sol phase was put into a thermostatic chamber at 308 K. After 24 h, 0.10 mL (1.10 mmol of H_2O) of the ethanol−water solution was further introduced and the addition was repeated every 24 h, until the desired value of the sol-phase viscosity was achieved. Three different viscosities were used for the spin-coating deposition: 1.4 cSt (24 h after the sol-phase preparation without any further addition of ethanol−water solution), 2.5 cSt (after five additions of 0.10-mL aliquots of ethanol−water solution), and 4.0−5.0 cSt (after seven additions of 0.10-mL aliquots of ethanol−water solution). In a similar way, pure SnO_2 films were obtained by the corresponding sol-phase solutions in the absence of Pt(II) acetylacetonate.

Both pure and Pt-doped SnO_2 films were deposited by spin-coating (spin rate = 2000 rpm) on (100) silicon wafers (0.6-mm thick, *p*-type SiCZ supplied by MEMC Electronic Material), then dried at room temperature, and finally annealed at 673 or 973 K in an air stream (80 cm^3 min^{-1}) for 2 h. As shown by our previous investigations,[14] at 473 K the acetylacetonate precursor was fully decomposed and no detectable organic residuals contaminated the grown films. The film thickness, measured by a Tencor P-10 surface profiler, is in the range 60−90 nm.

Film Characterization. The SNOM apparatus uses an illumination/reflection configuration where the light illuminated the sample from the fiber tip aperture (near field) and after reflection it is collected by a far-field device (phototube). Light source is a laser diode (λ = 650 nm, P_{max} = 3 mW) coupled to a monomodal optical fiber probe with a tip diameter

(14) Canevali, C.; Chiodini, N.; Morazzoni, F.; Scotti, R. *J. Mater. Chem.* **2000**, *10*, 773−778.
(15) Morazzoni, F.; Canevali, C.; Chiodini, N.; Mari, C.; Ruffo, R.; Scotti, R.; Armelao, L.; Tondello, E.; Depero, L. E.; Bontempi, E. *Chem. Mater.* **2001**, *13*, 4355−4361.
(16) Morimitsu, M.; Ozaki, Y.; Suzuki, S.; Matsunaga, M. *Sensors Actuators B* **2000**, *67*, 184.
(17) Diéguez, A.; Romano-Rodriguez, A.; Morante, J. R.; Weimar, U.; Schweizer-Berberich, M.; Gopel, W. *Sensors Actuators B* **1996**, *31*, 1.
(18) Kim, K. H.; Park, C. G. *J. Electrochem. Soc.* **1991**, *138*, 2408−2412.
(19) Bruno, L.; Pijolat, C.; Lalauze, R. *Sensors Actuators B* **1994**, *18−19*, 195−199.
(20) Barreca, D.; Garon, S.; Zanella, P.; Tondello, E. *J. Phys. IV France* **1999**, *9*, 667.
(21) Gaggiotti, G.; Galdikas, A.; Kačiulis S.; Mattogno, G.; Setkus, A. *Sensors Actuators B* **1995**, *24−25*, 516−519.
(22) Mochida, T.; Kikuchi, T.; Kondo, T.; Ueno, H.; Matsuura, Y. *Sensors Actuators B* **1995**, *24−25*, 433−437.
(23) Williams, G.; Coles, G. S. V. *MRS Bull.* **1999**, *24* (6), 25−29.
(24) Tokahashi, Y.; Wada, Y. *J. Electrochem. Soc.* **1990**, *137*, 267−272.
(25) Racheva, T. M.; Critchlow, G. W. *Thin Solid Films* **1997**, *292*, 299−302.
(26) Ivanovskaya, M. I.; Bogdanov, P. A.; Orlik, D. R.; Gurlo, A. C.; Romanovskaya, V. V. *Thin Solid Films* **1997**, *296*, 41−43.
(27) Cobianu, C.; Savianu, C.; Buiu, O.; Dascalu, D.; Zaharescu, M.; Parlog, C.; van den Berg, A.; Pecz, B. *Sensors Actuators B* **1997**, *43*, 114−120.
(28) Rella, R.; Serra, A.; Siciliano, P.; Vasanelli, L.; De, G.; Licciulli, A. *Thin Solid Films* **1997**, *304*, 339−343.
(29) Savianu, C.; Arnautu, A.; Cobianu, C.; Craciun, G.; Fueraru, C.; Zaharescu, M.; Parlog, C.; Paszti, F.; van den Berg, A. *Thin Solid Films* **1999**, *349*, 29−35.
(30) Brinker, C. J.; Scherer, G. W. In *Sol−Gel Science: The Physics and Chemistry of Sol−Gel Processing*; Academic Press: New York, 1990.
(31) Betzig, E.; Trautman, J. K.; Harris, T. D.; Weiner, J. S.; Kostelak, R. L. *Science* **1991**, *251*, 1468.
(32) Kirstein, S. *Curr. Opin. Colloid Interface Sci.* **1999**, *4*, 256.
(33) Hampden-Smith, M. J.; Wark, T. A.; Rheingold, A.; Huffman, J. C. *Can. J. Chem.* **1991**, *69*, 121.

of about 50 nm. The detection of shear forces between the sample and the probe acts as regulation method to keep constant, and usually <10 nm, the distance between them. A piezoelectric tuning fork sensing element has the optical fiber tip attached along one of the tines of the fork itself, oriented so that the tip vibrates (with a resonance frequency of 34 kHz) parallel to the surface of the sample. In this control scheme, the feedback signal is produced by a change in amplitude of vibration of the system fork/fiber as the fiber tip approaches the sample and its value, collected during the mapping of the sample by an *xyz* piezo stage, can be considered a measure of the local surface topography. This configuration allows one to obtain simultaneously decoupled topographic and optical contrast images at the same time. Light scattered by the sample is collected by a 20× objective and sent, through an interference filter ($\lambda = 650$ nm, fwhm=10 nm), to a high-gain photomultiplier tube.

AFM micrographs were taken using a Park Autoprobe CP instrument operating in air in contact mode with a 5-μm scanner. The background was subtracted from the images using the ProScan 1.3 software supplied by Park Scientific. Different areas of each sample surface were analyzed to test the film homogeneity. SEM micrographs were taken by a Cambridge MK2 250 stereoscan instrument.

The GIXRD (glancing incidence X-ray diffraction) data were collected by a Bruker "D8 Advance" diffractometer equipped with a Göbel mirror. The angular accuracy was 0.001° and the angular resolution was better than 0.01°. The Cu Kα line of a conventional X-ray source powered at 40 kV and 40 mA was used for the experiments. The average crystallite dimensions were evaluated by means of the Scherrer equation. A similar apparatus, equipped with the general area detector diffraction solution (GADDS), was used to collect the microdiffraction data.

Electrical measurements were performed on 10 × 10 mm thin films deposited on Suprasil quartz glass plates. Two gold layers, 10 × 4 mm, were deposited on thin films at a distance of 2 mm from each other, by dc sputtering technique. Such procedure was carried out on films annealed at 673 and 973 K in a synthetic air stream (10 l h^{-1}) for 2 h. The samples were put in a quartz glass chamber and then placed in an oven and the sensitivity was measured as a function of the temperature (373−623 K). The electrical resistance was measured by a Keithley 617 programmable electrometer using the standard constant current method. The data acquisition was performed by a PC connected to the electrometer.

The sensing element was equilibrated in an air stream (10 L h^{-1}), then a CO (800 ppm)/air mixture was introduced (10 L h^{-1}), and the resistance was recorded until equilibrium conditions were reached. The initial conditions of the film were restored by air equilibration, before introducing again the CO/air mixture. Such procedure was repeated several times. The results of electrical characterization are reported as sensitivity $S = R_{air}/R_{CO}$, where R_{air} and R_{CO} stand for the resistance values in air and CO/air, respectively.

Results and Discussion

Morphology: SNOM, AFM, and SEM Investigation. Preliminary morphological investigations were performed on SnO_2 and Pt − doped SnO_2 thin films, deposited from a 2.5 cSt viscosity sol, and then annealed in air at 673 and 973 K. Table 1 reports the analyzed samples and the corresponding annealing temperatures, together with the average surface roughness as evaluated by AFM (see below).

The SNOM images reveal that film morphology depends on the chemical composition and thermal processing. Irrespective of the annealing temperature, pure SnO_2 coatings do not show detectable cracks, holes, or grains (see Sn973 as an example in Figure 1a). Conversely, in Pt-doped SnO_2 films annealed at 673 K, PtSn673 (Figure 1b), holes (darker areas in the figure), distributed throughout the film surface, can be clearly evidenced. The average hole diameter and depth are ≈400 and 50 nm, respectively. After annealing at 973 K, PtSn973 sample, most of the holes are filled by spherical particles (brighter areas) (Figure 1c), which give an optical response different from that obtained by the smooth areas.

Table 1. Morphological Parameters Obtained from AFM and SEM Analysis

sample		annealing temp (K)	average roughness from AFM[a] (nm)	R^b from SEM 1.4 cSt	2.5 cSt	4.0−5.0 cSt
SnO_2	Sn673	673	3.2	n.d.[c]	n.d.[c]	0.040
	Sn973	973	3.5			
Pt:SnO_2	PtSn673	673	6.0	0.010	0.028	0.074
	PtSn973	973	2.7			

[a] From 2.5 cSt sol-phase. [b] Ratio between the area of the surface hole section and the total area of films deposited from different viscosity sols. [c] Not determined as holes are subsurface located.

To attain deeper insight about the influence of the doping element and the annealing treatments on the film morphology, AFM micrographs of all the samples were recorded and associated with SNOM images (Figure 1). Micrographs are in good agreement with SNOM results. In fact, pure SnO_2 films show regular and smooth surfaces irrespective of the treatment temperature (Figure 1a for sample Sn973), with an average surface roughness of ≈3.5 nm. Conversely, holes with an average diameter of about 400 nm are clearly detected on the surface of PtSn673 samples (Figure 1b), whose average surface roughness accordingly increases to 6 nm. In PtSn973 coatings (Figure 1c), the holes appear often filled by globular extrusions with a central hole. This filling reduces the average roughness to 2.7 nm (see Table 1).

The hypothesis that the doping metal induces variations in the surface roughness and the formation of large holes was tested in a large area by performing a systematic scanning electron microscopy (SEM) analysis on samples obtained from three different viscosity sols, dried at room temperature, and annealed at 673 K. The results are reported in Figure 2.

At variance with what observed by AFM and SNOM analyses, also the undoped SnO_2 films show a high density of defects. These defects are generally observed in backscattering mode in SnO_2 layers derived from lower viscosity sol (1.4 and 2.5 cSt); in samples obtained from high-viscosity sol (5.0 cSt), holes were detected also by secondary electrons. These findings suggest that holes of two different types can be distinguished by SEM analysis of SnO_2 films: those located on the sample surface and those lying in a subsurface region which are only visible in backscattering mode. The average hole dimension as well as the number of surface-located holes increase as a function of the sol precursor viscosity. Conversely, no relevant differences are observed between the room-temperature dried and 673 K annealed films. Larger holes are observed for Pt-doped SnO_2 where the sample defectivity increases on going from the room-temperature dried layers to the 673 K annealed films. The defects in Pt-doped films are located both at the surface and in the subsurface region for each sol precursor viscosity.

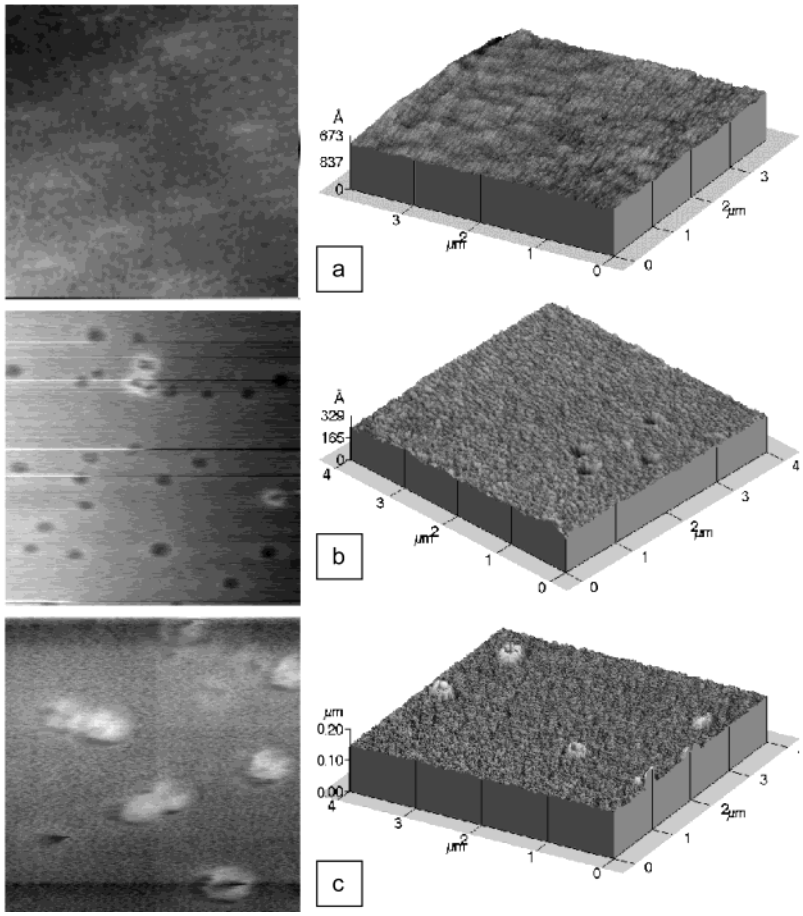

Figure 1. Topographic SNOM maps ($10 \times 10\ \mu m^2$) (left) and AFM surface micrographs ($4 \times 4\ \mu m^2$) (right) of samples (a) Sn973, (b) PtSn673, and (c) PtSn973 on Si substrate.

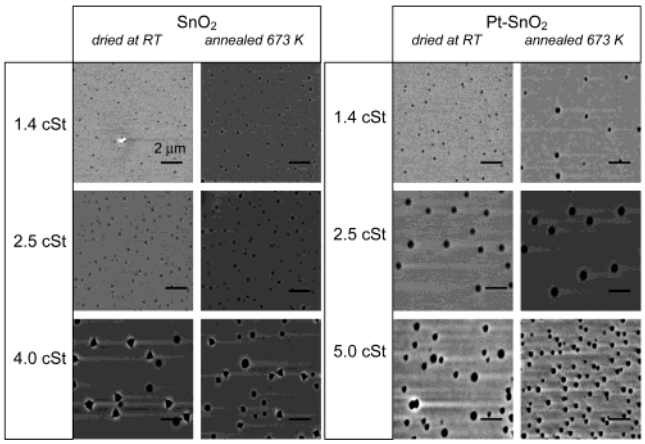

Figure 2. SEM micrographs of pure SnO_2 and Pt-doped SnO_2 films, deposited at different viscosities (indicated in figure), dried at room temperature, and annealed at 673 K.

SEM-EDX analyses were performed on PtSn673 and PtSn973 samples to investigate whether the defects have a different elemental composition with respect to the smooth film surface. To this regard, no differences were found.

Microstructure: GIXRD and Microdiffraction Investigations. The GIXRD study on SnO_2 and Pt-doped SnO_2 films obtained from a 2.5 cSt viscosity sol precursor at an incidence angle of 1° was already reported.[15] All these samples show the cassiterite structure. It was reported[15] that the average crystallite size of pure and Pt-doped SnO_2 films increases from 3 to 6 nm, for annealing temperatures ranging from 673 to 973 K. In addition the presence of platinum in the SnO_2 coatings affects the intensity of the cassiterite reflections at $2\theta = 52°$ and $2\theta = 54.5°$ (JSPDS, card no. 721147) when the annealing temperature is raised from 673 to 973 K.[15] New analyses, performed with a D8 Advance microdiffractometer equipped with the GADDS area detector at a fixed incidence angle of 0.2°, exclude any preferred orientation of the films. In fact, no significant differences were observed in the intensities along the Debye rings. Moreover, the integration of the 2D diffraction pattern confirmed the difference in the intensities ratio of the cassiterite phase with respect to the ideal structure, already observed[15] for different annealing temperatures of Pt-doped SnO_2 coatings. A new phase, probably a platinum oxide (PtO_x) segregated in the outermost layers, was re-confirmed as being responsible for the changes in the relative intensities of the peaks at 52° and 54.5° in the PtSn973 sample. A more precise structural identification of the segregated phase was prevented by the existence of a few Pt oxides with strong diffraction lines in the range of 50°−55°.

Similar results were obtained on thin films deposited from 1.4, 2.5, and 5.0 cSt sol-precursor viscosities. These findings suggest that the microstructure is not dependent on the sol viscosity.

Electrical Investigation. In a previous paper[15] we discussed the sensing behavior toward the CO/air atmosphere of Pt-doped SnO_2 films and the results were

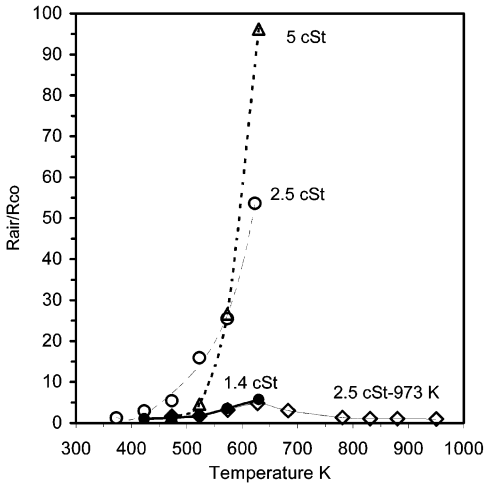

Figure 3. Plot of sensitivity (R_{air}/R_{CO}) in CO (800 ppm)/air stream vs temperature for Pt-doped SnO_2 films, deposited at different viscosities and annealed at 673 K. Sensitivity of Pt-doped SnO_2 films, deposited at viscosity 2.5 cSt and annealed at 973 K, is also reported.

compared with that of pure SnO_2 coatings. We reported that the sensitivity values, in the 373−973 K temperature range, depended on the annealing temperature. In particular, the film deposited from a 2.5 cSt viscosity sol and annealed at 673 K (PtSn673) showed a sensitivity value 10 times higher than that observed for the PtSn973 one.

The sensitivity of the Pt-doped SnO_2 films, deposited from different viscosity sols, is now reported in Figure 3. For all the films the sensitivity increases as a function of the working temperature, but it is very low in films deposited from the lowest viscosity sol (1.4 cSt). The highest sensitivity was measured for samples obtained from the highest viscosity sol (5.0 cSt).

Considering the results of the morphological investigation reported in the present paper for PtSn673 samples obtained from different viscosity sols, it seems that the presence of holes on the film surface, far from inhibiting the electrical transport, promotes the electronic exchange at the surface. It could be hypothesized that the hole effect was that of increasing the surface area. Since surface area measurements cannot be accurately performed in the case of thin films, we evaluated, through SEM image analysis, the ratio between the area of the surface hole section and the total area of the films deposited from different viscosity sols and annealed at 673 K (*R* parameter in Table 1). *R* values display a similar trend to that shown by highest sensitivity values of the corresponding films, although a linear correlation was not found nor expected. Consequently, the enhanced sensitivity was ascribed to the morphology of the layers and in particular to the increase in surface area due to the presence of holes. However, effects associated with bulk porosity cannot be excluded.

At higher annealing temperature (973 K), the increased mobility of the atoms gives rise to the formation of extrusions, partially filling the surface holes. This effect, besides the doubling of the grain dimension and the decrease of surface area, can be considered coresponsible for inhibiting the electrical transport in PtSn973 films with respect to PtSn673 samples (Figure 3). In fact, extrusions can create an energy barrier toward the electrical transport at the defect boundary. PtO_x phases, segregated at the surface and not detectable by EDX analysis, could also contribute to a decrease in the electrical sensitivity.

Conclusion

This work has focused on the morphological analysis of nanostructured SnO_2 and Pt-doped SnO_2 thin films to be used for CO gas sensor devices. Following our previous investigation on the microstructural, electronic, and magnetic properties,[15,34] the present paper was aimed at evaluating the influence of morphological characteristics on the film electrical sensitivity.

The obtained results show that the surface morphology, characterized by the presence of holes, was mainly dependent on the sol-precursor viscosity, on the dopant presence, and on the annealing temperature (673 or 973 K). Concerning hole formation, it could be hypothesized that the surface tension of the sol phase increased as a function of viscosity and platinum doping. A higher surface tension might have caused a more difficult release of the residual gases during film drying and annealing; hence, the largest and deepest holes are expected to be formed in Pt-doped films deposited from higher viscosity sols.

As shown by the present investigation, the preparation of long-term reproducible sensing films based on Pt-doped SnO_2 relies on fine and tailored control of the defect morphology.

On the basis of our results, high-sensitivity small-sized Pt-doped SnO_2 devices may be obtained by sol−gel provided that samples are prepared from high-viscosity sol precursors and annealed at a temperature as low as 673 K.

Acknowledgment. The authors are grateful to APE Research for SNOM analysis and Bruker AXS access to Karlsruhe (Germany) Laboratories. Progetto Finalizzato “Materiali Speciali per Tecnologie Avanzate II” financially assisted this work.

CM031002W

(34) Armelao, L.; Barreca, D.; Bontempi, E.; Canevali, C.; Depero, L. E.; Mari, C.; Ruffo, R.; Scotti, R.; Tondello, E.; Morazzoni, F. *Appl. Magn. Reson.* **2002**, *22*, 89−100.